Supporting Information

Two-dimensional Cobalt Telluride as Piezo-tribogenerator

Solomon Demiss[a,b]‡, Raphael Tromer[c]‡, Chinmayee Chowde Gowda[d], Cristiano F. Woellner[e], Olu Emmanuel Femi[b], Ajit K. Roy[f], Prafull Pandey[g], Douglas S. Galvao[c,h]*, Pulickel M. Ajayan[i]*, Partha Kumbhakar[a]*, Chandra Sekhar Tiwary[b]*

[a]Department of Metallurgical and Materials Engineering, Indian Institute of Technology Kharagpur, West Bengal, 721302 India.

[b]Materials Science and Engineering, Jimma Institute of Technology, Jimma University, Jimma, Ethiopia.

[c]Applied Physics Department, University of Campinas, Brazil.

[d]School of Nano Science and Technology, Indian Institute of Technology Kharagpur, West Bengal, 721302 India.

[e]Physics Department, Federal University of Parana, UFPR, Curitiba, PR, 81531-980, Brazil

[f]Materials and Manufacturing Directorate, Air Force Research Laboratory, Wright Patterson AFB, OH 45433-7718, United States.

[g]Department of Materials Engineering, Indian Institute of Science, Bangalore 560012, India.

[h]Center for Computational Engineering and Sciences, State University of Campinas, Campinas, SP, 13083-970, Brazil.

[i]Department of Materials Science and Nano Engineering, Rice University, Houston, TX 77005, USA

Corresponding Author

*Email addresses - galvao@ifi.unicamp.br, parthakumbhakar2@gmail.com, ajayan@rice.edu, chandra.tiwary@metal.iitkgp.ac.in,

Experimental Section

The output voltage from the devices under mechanical load and applied heat were measured under different resistances. Similarly, power output was also calculated from these results. After making the device using the spin-coating method, AFM measurements have been carried out. From the results (see **Figure S14**), we have shown that most of the sheets are distributed throughout the substrate. Since we observe multiple layers with also some of them overlapping, we can confirm that the most oriented flakes are in one direction in order to obtain maximum efficiency. Therefore, the cancelation of the piezoelectric property of the $CoTe_2$ sheets due to overlapping is negligible. SEM image was also done for the cell to observe the coating of the sample (**Figure S15**). The mechanical force was applied on these flexible nanogenerators by finger tapping, hitting with constant pressure, and bending (**Figure S16**).

Detailed calculation of power and energy conversion efficiency of PTNG cell:

Output power of the cell:

The maximum power output (P) for a cell of 9 cm^2 area was calculated using equation (1) as mentioned below,

$$P = \frac{1}{A}\frac{V^2}{R_L} \quad (1)$$

where A is the surface area (9 cm^2) of PTNG, Vo is the maximum output voltage (~5V) and R is load resistance of the circuit which was calculated from a rectifier circuit and is 9 MΩ [1].

Energy conversion efficiency of the cell:

The energy conversion efficiency can be obtained by the ratio of output electrical energy (E_{elec}) and input mechanical energy (E_{mech}) [2]

$$\eta = \frac{E_{elec}}{E_{mech}} \quad (2)$$

Further output electrical energy for each cycle of the PTNG was calculated using the formula

$$E_{elec} = \int \frac{V(t)^2\, dt}{R} \quad (3)$$

where V(t) is the output voltage and R is the the load resistance of ~9 MΩ. The values for varied temperatures are tabulated in **Table S1**. Similarly, input mechanical energy was calculated using the formula,

$$E_{mech} = F\varepsilon t \quad (4)$$

where F is applied force 1N, *t* is the thickness of the substrate 0.6 mm and ε is the axial strain in the PTNG.

Current density of the cell at varying temperatures:

From theoritical calculations we were able to deduce piezoelectric coefficients (**Table 1**) for temperatures 300 K and 320 K. Equation for current density is as shown below

$$I_{sc} = \frac{4fV_{oc}d_{ij}}{Lg_{3j}} \quad (5)$$

The values suggest that the current density increases with increasing temperature. With this we can concur that the cell can be used to monitor temperature fluctuations in the range of 300 to 320 K and can be implemented on a working electronic device (laptop in our case) to sense overheating temperatures.

Charge generation mechanism:

A net polarization and charge generation was obtained. When the pressure was applied, the dipolar momentum and overall polarization in the pressed state is changed from the initial state; thus an electric current (I_P) is generated as a response to the induced applied pressure. After that, when the pressure is released, the opposite electrical potential change is induced, and the structure returns to its original state. The output electrical potential depends on the deformation of the lattice structure of $CoTe_2$, and it is due to the applied stress, as charges appear on the opposite faces in the 2D $CoTe_2$. The figure also shows the triboelectric model, which depicts

the generation of charges through a triboelectric effect in two materials with a difference in electron affinities. The change in the electrostatic momentum is obtained when two charged materials under applied pressure produce a change in electrical potential

Supporting Figures

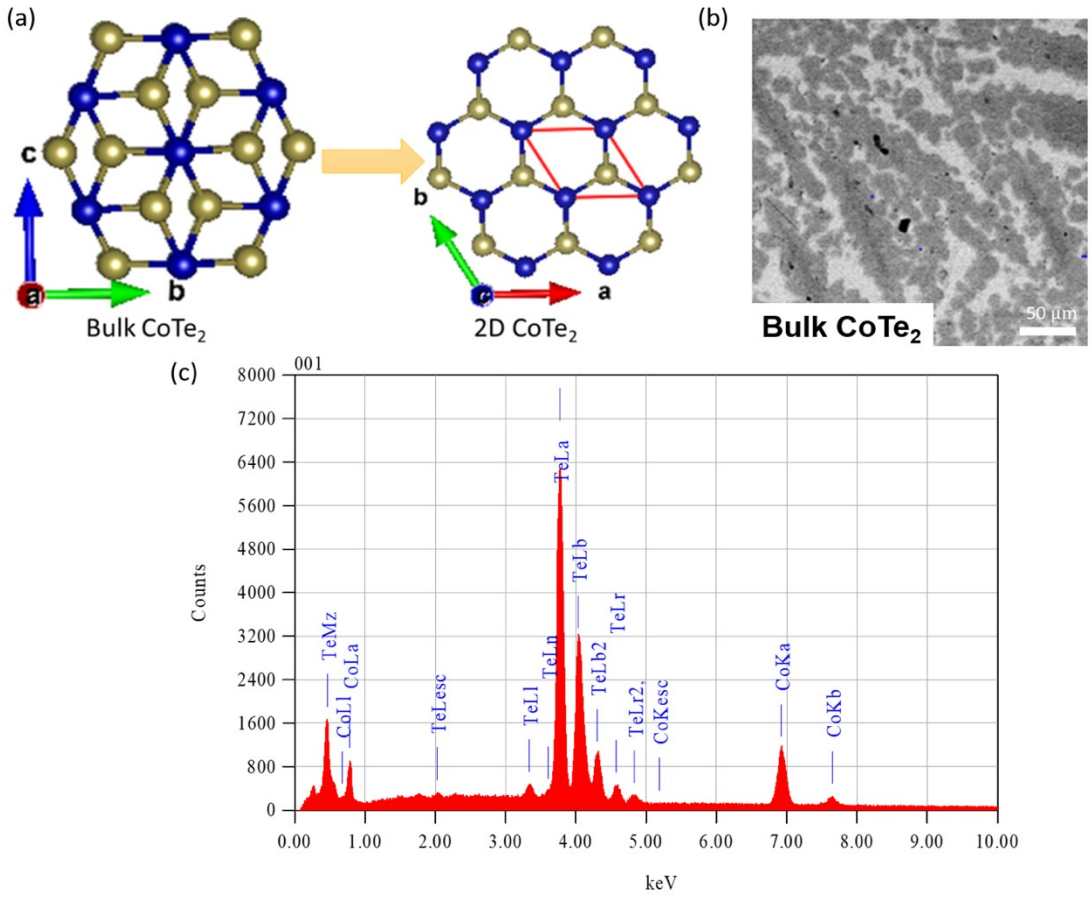

Fig. S1: (a) Phase transition observed in exfoliated crystal structure, (b) SEM image and (c) EDX compositional analysis of Bulk $CoTe_2$.

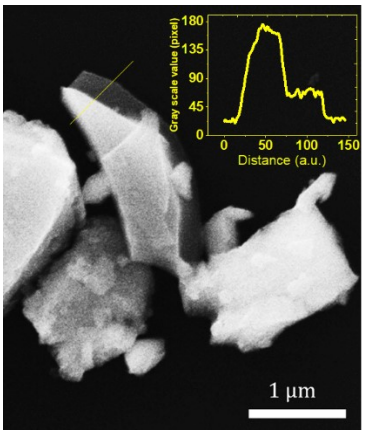

Fig. S2: SEM image of exfoliated layered $CoTe_2$ with multilayer stacks. The inset shows the optical contrast as a function of the thickness of the sample, measured using a line scan profile (grayscale value).

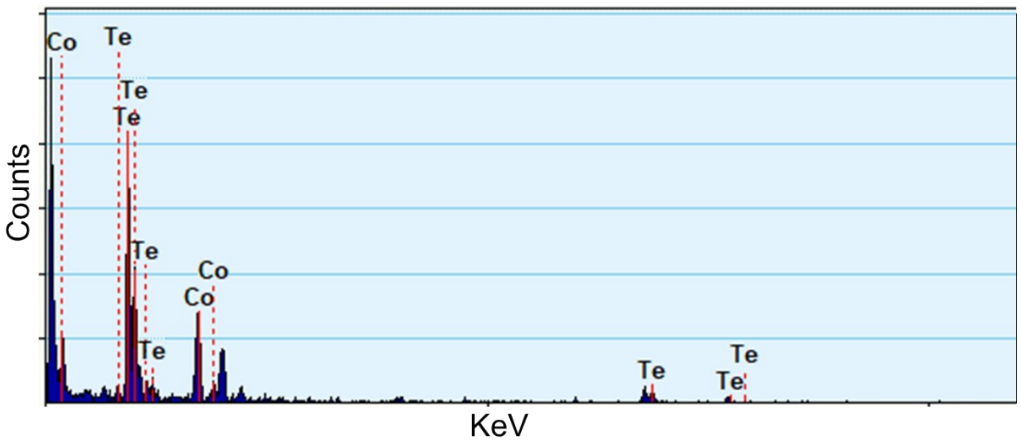

Fig. S3: Elemental composition analysis by EDX of 2D $CoTe_2$.

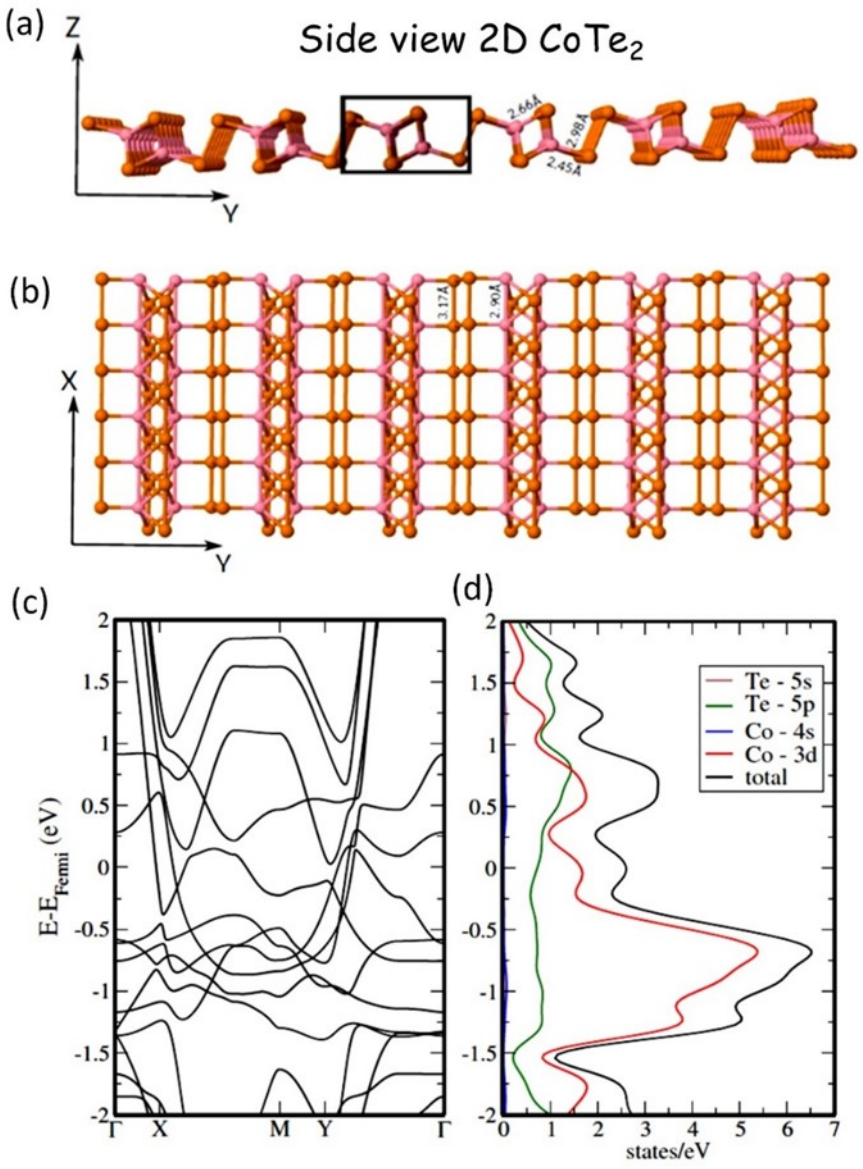

Fig. S4. (a) Side view and (b) Front views of the optimized structure of 2D $CoTe_2$ exfoliated at the [120] crystal direction from $CoTe_2$ bulk, (c) Electronic band structure, and (d) the corresponding projected density of states (PDOS) of the structure.

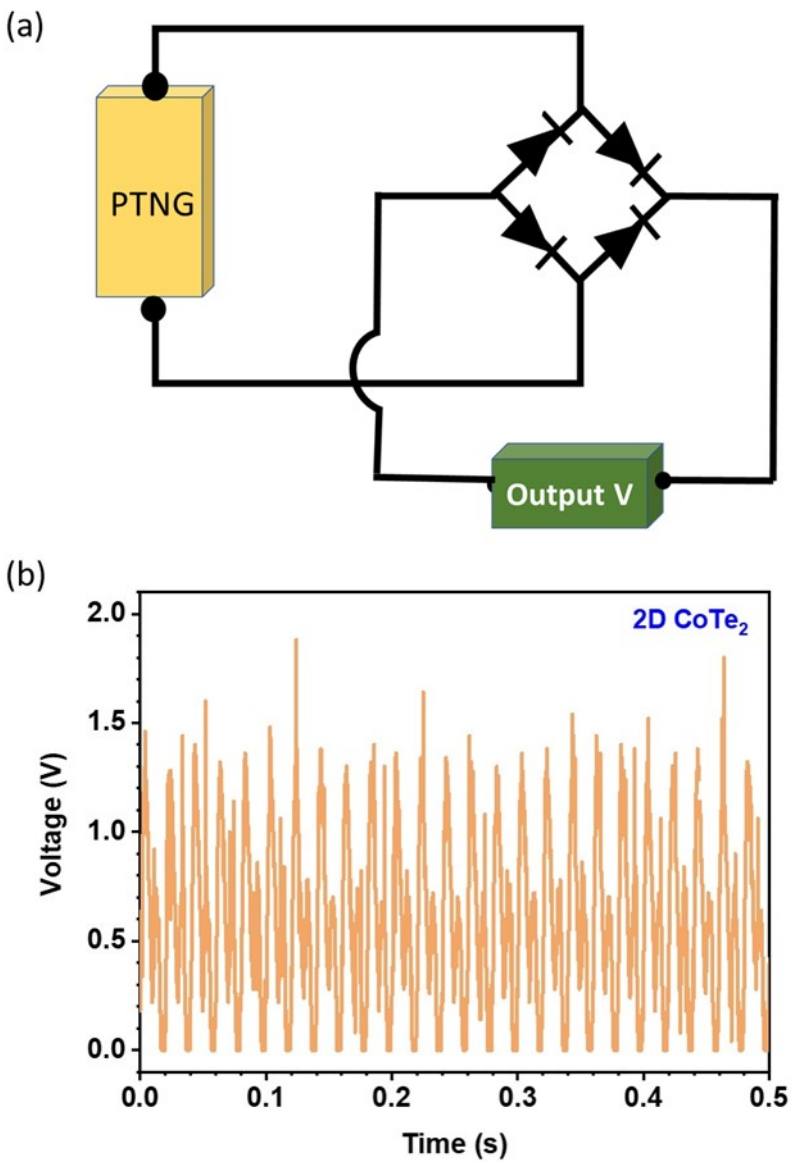

Fig. S5: (a) Circuit diagram of bridge rectifier circuit and (b) Hybrid cell output across bridge rectifier circuit, positive cycle voltage output

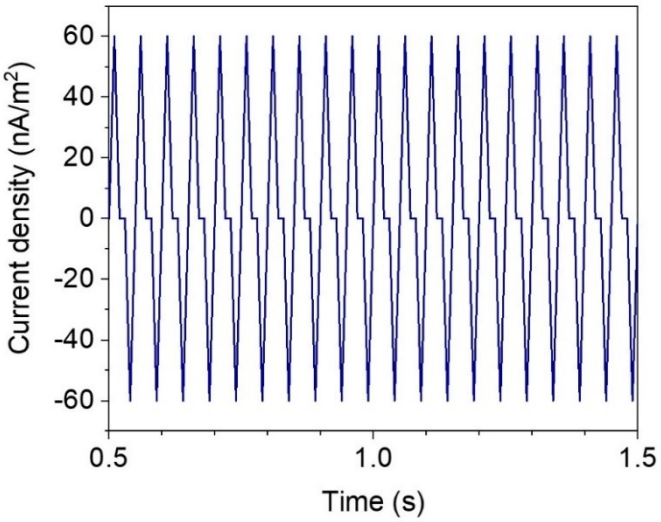

Fig. S6: Current density of PTNG cell under continuous pressure.

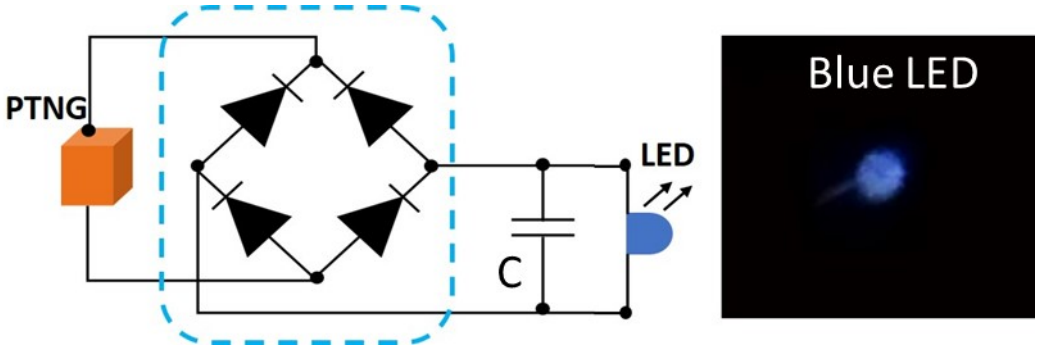

Fig. S7. LED was lit up using the PTNG cell.

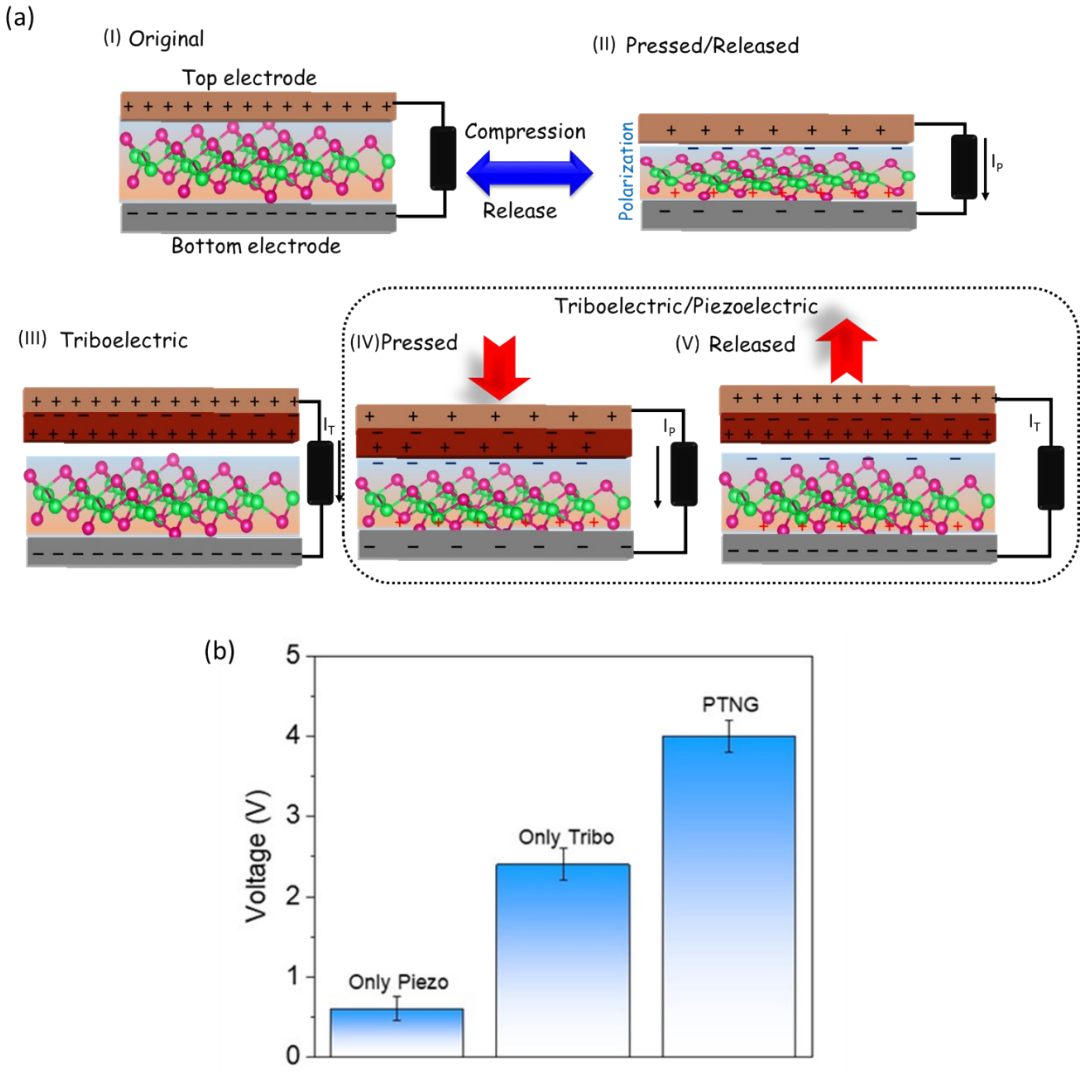

Fig. S8: (a) Proposed schematic representation of (I, II) piezoelectric, (III) triboelectric and combined (IV-V) piezo-tribo response of the hybrid cell. (b) Contributions of different mechanisms affecting charge generation in PTNG cells.

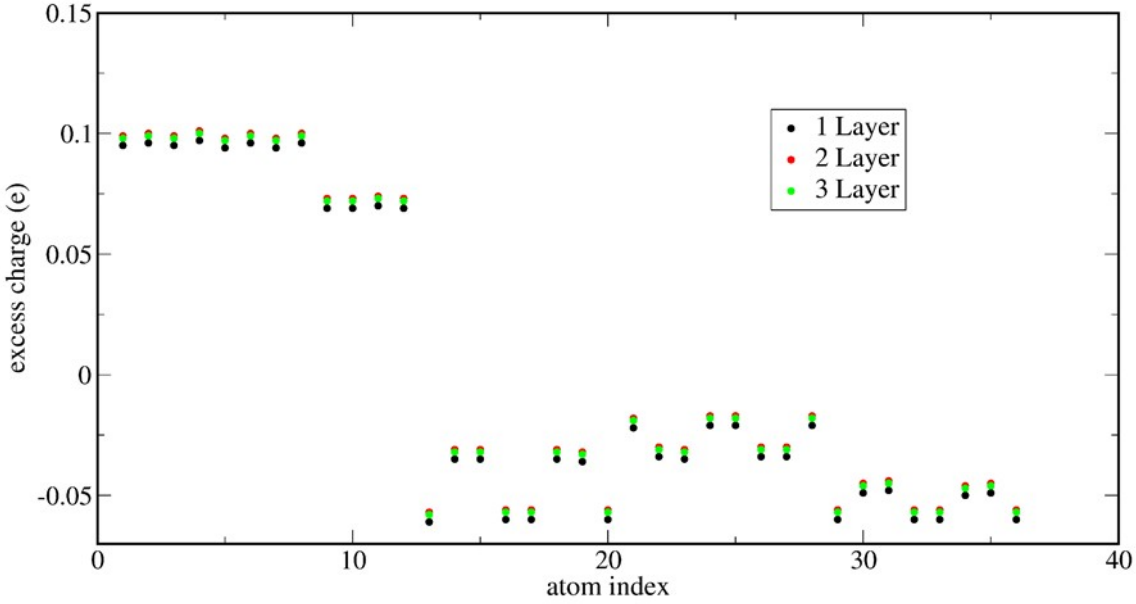

Fig. S9. Surface charge as a function of layer number

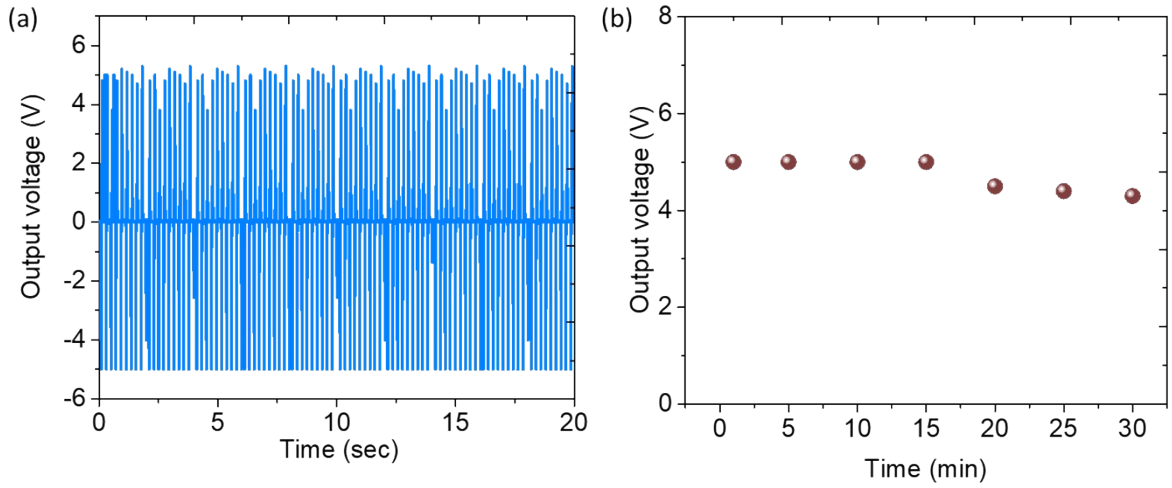

Fig. S10. (a) Output performance under continuous pressure on the cell and (b) Stability of the cell after 30 min of continuous pressing.

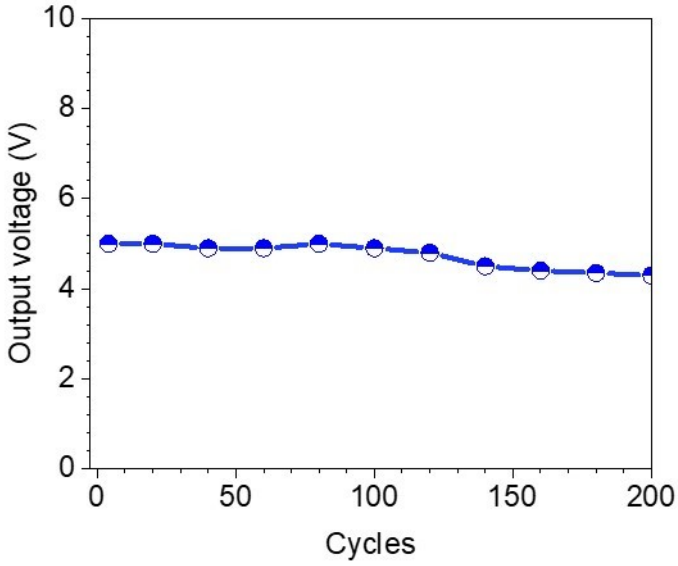

Fig S11: Fatigue test of PTNG cell

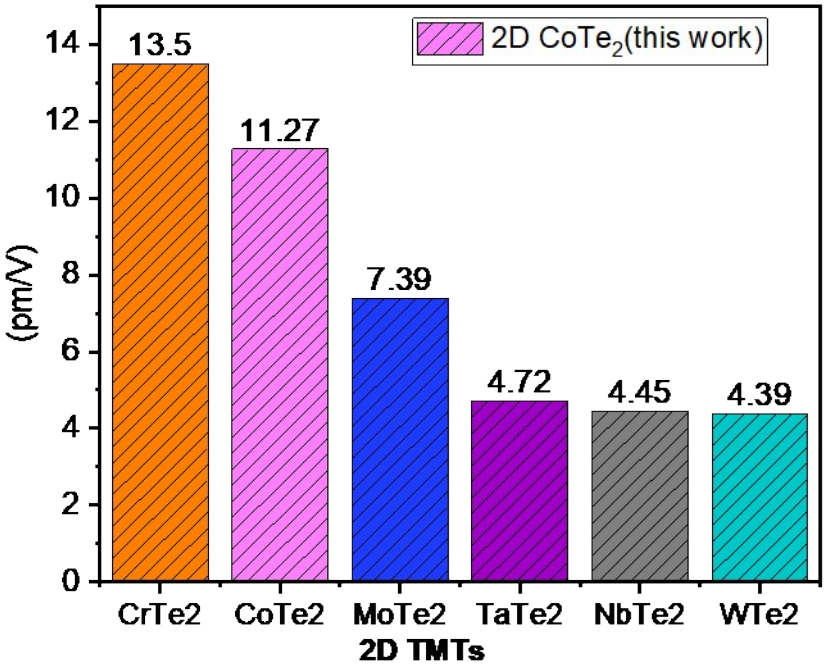

Fig. S12. Comparison graph for piezo-coefficient [S3, S8]

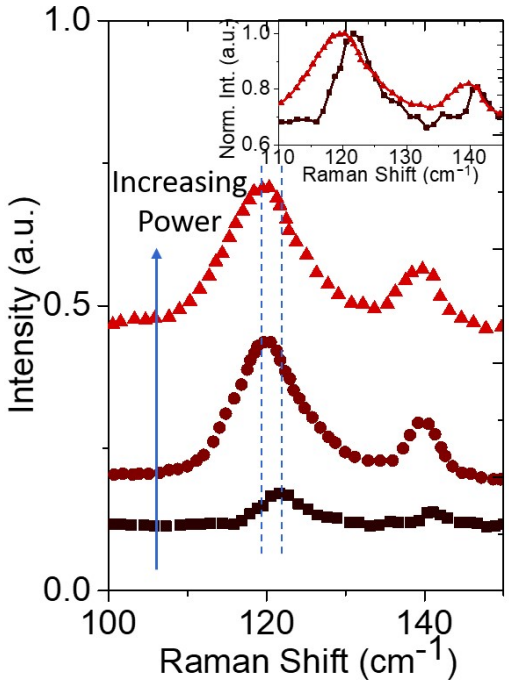

Fig. S13: Laser power dependent Raman spectra and lines indicating the shifting of Raman mode.

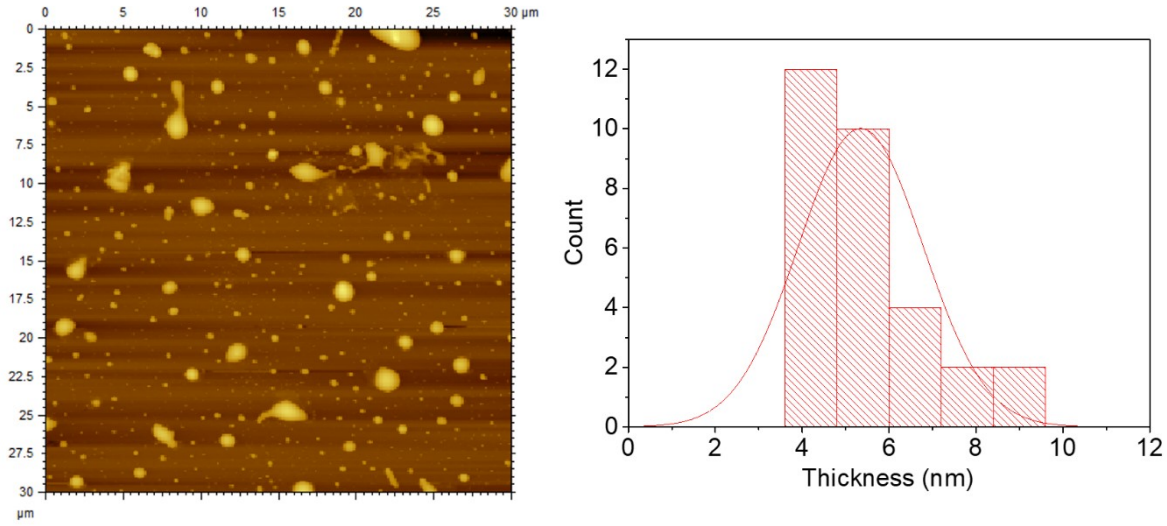

Fig. S14. Typical AFM image and the corresponding estimated thickness of the $CoTe_2$ samples in the PTNG cell.

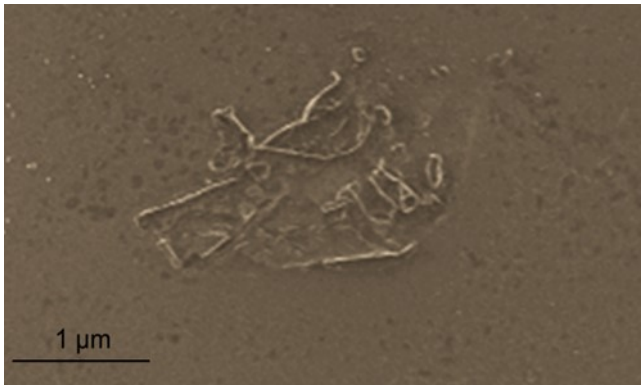

Fig. S15: SEM image of the cell

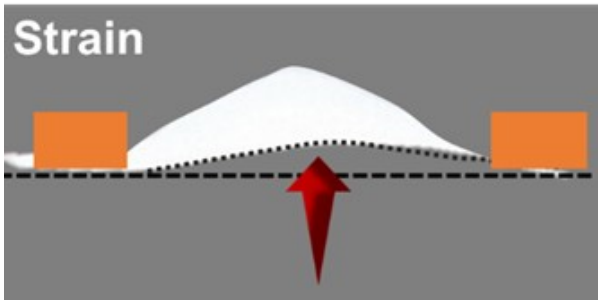

Fig. S16: Schematic of cell bending

Table S1: Efficiency calculation at different tempertaure conditions

Temperature (K)	E_{elec} (J)	E_{mech} (J)	η (%)
304	2.6×10^{-8}	5.24×10^{-7}	7.96
311	7.8×10^{-8}		14.89
321	9.7×10^{-8}		18.51
343	1×10^{-7}		19.08
363	1.12×10^{-7}		21.37

Reference:

[S1] S. K. Ghosh, P. Adhikary, S. Jana, A. Biswas, V. Sencadas, S. D. Gupta, B. Tudu, D. Mandal, Electrospun Gelatin Nanofiber Based Self-Powered Bio-e Skin for Health Care Monitoring, *Nano Energy*, **2017,** 36, 166-175.

[S2] K. Maity, S. Garain, K. Henkel, D. Schmeißer, D. Mandal, Self-Powered Human-Health Monitoring through Aligned PVDF Nanofibers Interfaced Skin-Interactive Piezoelectric Sensor, *ACS Appl. Polym. Mater*. **2020**, 2, 862–878.

[S3] Cui, C., Xue, F., Hu, WJ. et al. Two-dimensional materials with piezoelectric and ferroelectric functionalities. npj 2D Mater Appl 2, 18 (2018). https://doi.org/10.1038/s41699-018-0063-5.

[S4] Su, J.; Liu, K.; Wang, F.; Jin, B.; Guo, Y.; Liu, G.; Li, H.; Zhai, T. Van der Waals 2D Transition Metal Tellurides. Adv. Mater. Interfaces 2019, 6, 1900741, 10.1002/admi.201900741

[S5] Huang, H.; Fan, X.; Singh, D. J.; Chen, H.; Jiang, Q.; Zheng, W. Controlling Phase Transition for Single-Layer MTe_2 (M= Mo and W): Modulation of the Potential Barrier under Strain. Phys. Chem. Chem. Phys. 2016, 18, 4086– 4094, 10.1039/C5CP06706E.

[S6] Balandin, A. A.; Ghosh, S.; Bao, W.; Calizo, I.; Teweldebrhan, D.; Miao, F.; Lau, C. N. Superior Thermal Conductivity of Single-Layer Graphene. Nano Lett. 2008, 8, 902– 907, 10.1021/nl0731872

[S7] Wang, Y.; Cong, C.; Qiu, C.; Yu, T. Raman Spectroscopy Study of Lattice Vibration and Crystallographic Orientation of Monolayer MoS_2 under Uniaxial Strain. Small 2013, 9, 2857–2861, 10.1002/smll.201202876

[S8] Blonsky, M. N.; Zhuang, H. L.; Singh, A. K.; Hennig, R. G. Ab Initio Prediction of Piezoelectricity in Two-Dimensional Materials, ACS Nano 2015, 9, 10, 9885–9891, https://doi.org/10.1021/acsnano.5b03394